Comparison Results of Three First-order Finite Element Methods for the Poisson Model Problem*

C. Carstensen [†⋆] D. Peterseim [†] M. Schedensack [†]

December 5, 2011

Abstract

This paper establishes the equivalence of conforming Courant finite element method and nonconforming Crouzeix-Raviart finite element method in the sense that the respective energy error norms are equivalent up to generic constants and higher-order data oscillations in a Poisson model problem. The Raviart-Thomas mixed finite element method is better than the previous two whereas the conjecture of the converse relation is proved to be false.
This paper completes the analysis of comparison initiated by Braess in Calcolo (2010). Two numerical benchmarks illustrate the comparison theorems and the possible strict superiority of the Raviart-Thomas mixed finite element method. Applications include least-squares finite element methods and equality of approximation classes for concepts of optimality for adaptive finite element methods.

Keywords finite element method, nonconforming FEM, Crouzeix-Raviart, Raviart-Thomas, least-squares method, approximation class.

AMS subject classifications 65N12, 65N30, 65Y20.

*This work is supported by the DFG Research Center Matheon Berlin and by the WCU program through KOSEF (R31-2008-000-10049-0).

†Institut für Mathematik, Humboldt-Universität zu Berlin, Unter den Linden 6, D-10099 Berlin, Germany

⋆Department of CSE, Yonsei University Seoul, Korea

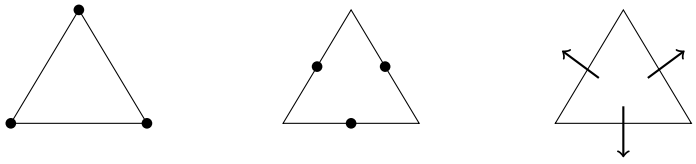

Figure 1.1: CFEM (left), CR-NCFEM (middle), RT-MFEM (right).

1 Introduction

Given a bounded polygonal domain Ω in the plane and data $f \in L^2(\Omega)$, the Poisson model problem seeks the weak solution $u \in H^1(\Omega)$ of

$$-\Delta u = f \text{ in } \Omega \text{ and } u = 0 \text{ on } \partial\Omega. \tag{1.1}$$

This paper compares the error of three popular finite element methods (FEM) for the numerical solution of (1.1) as depicted in Figure 1.1, the conforming *Courant* FEM (CFEM) [11], the nonconforming *Crouzeix-Raviart* FEM (CR-NCFEM) [12], and the mixed *Raviart-Thomas* FEM (RT-MFEM) [18] with respective solutions u_{C}, u_{CR}, and $(p_{\mathrm{RT}}, u_{\mathrm{RT}})$ based on a shape-regular triangulation of Ω.

As the main result (in Theorems 1 and 2) we will show that

$$\|\nabla u - p_{\mathrm{RT}}\|_{L^2(\Omega)} \lesssim \|\nabla_{\mathrm{NC}}(u - u_{\mathrm{CR}})\|_{L^2(\Omega)} \approx \|\nabla(u - u_{\mathrm{C}})\|_{L^2(\Omega)} \tag{1.2}$$

holds up to data oscillation $\operatorname{osc}(f, \mathcal{T})$ and up to mesh-size independent generic multiplicative constants (hidden in the notation $\lesssim$ and $\approx$). The conjecture

$$\|\nabla_{\mathrm{NC}}(u - u_{\mathrm{CR}})\|_{L^2(\Omega)} \lesssim \|\nabla u - p_{\mathrm{RT}}\|_{L^2(\Omega)}$$

is false in general (Theorem 3). It is remarkable that those results do *not* rely on the regularity of the solution u.

A comparison of the methods under consideration has been initiated in [5], where the hypercircle method proves $\|\nabla u - p_{\mathrm{RT}}\| \lesssim \|\nabla_{\mathrm{NC}}(u - u_{\mathrm{CR}})\| \lesssim \|\nabla(u - u_{\mathrm{C}})\|$. This paper gives direct proofs and a throughout comparison. The novel result

$$\|\nabla_{\mathrm{NC}}(u - u_{\mathrm{CR}})\|_{L^2(\Omega)} \lesssim \|p - \Pi_0 p\|_{L^2(\Omega)} + \operatorname{osc}(f, \mathcal{T}) \tag{1.3}$$

from [14, Section 3.1] with the L^2 projection of the flux $p := \nabla u$ onto its piecewise constant integral means $\Pi_0 p$ leads to a third proof of $\|\nabla_{\mathrm{NC}}(u - u_{\mathrm{CR}})\|_{L^2(\Omega)} \lesssim \|\nabla(u - u_{\mathrm{C}})\|_{L^2(\Omega)}$ with other tools.

An immediate application to least-squares finite element methods improves a comparison result of [15] and disproves a further conjecture. The comparison results also clarify that various approximation classes for the optimality of adaptive FEM coincide.

The outline of this paper is as follows. Section 2 introduces the precise notation and states the main results in Theorems 1, 2, and 3 and comments on it. Section 3 gives their proofs based on arguments from the a posteriori error analysis. Section 4 illustrates the equivalences in a typical situation and in the context of the counterexample of Theorem 3 below. The arguments are expected to be possibly generalised to further applications and numerical schemes as well as to higher dimensions and more general boundary conditions.

Throughout this paper, standard notation on Lebesgue and Sobolev spaces is employed and $A \lesssim B$ abbreviates an inequality $A \leq C\,B$ with some mesh-size independent generic constant $0 \leq C < \infty$; $A \approx B$ abbreviates $A \lesssim B \lesssim A$. All hidden generic factors depend on a lower bound of the minimal angle in $\mathcal{T}$.

2 Results

2.1 Three Finite Element Methods

This section defines the three finite element methods of Figure 1.1 and states the main results of this paper. The proofs follow in the subsequent section.

Let $\mathcal{T}$ denote a shape-regular triangulation of a polygonal bounded Lipschitz domain Ω into (closed) triangles, i.e., $\bar{\Omega} = \cup\mathcal{T}$ and any two elements are either disjoint or share exactly one edge or share exactly one vertex. Let $h_{\mathcal{T}} \in P_0(\mathcal{T})$ denote the $\mathcal{T}$-piecewise constant mesh width function with $h_{\mathcal{T}}|_T = \operatorname{diam}(T)$ for all $T \in \mathcal{T}$. Let $\mathcal{E}$ denote the set of edges of $\mathcal{T}$ and $\mathcal{N}$ the set of vertices, $\mathcal{N}(\Omega)$ denotes the interior nodes. Throughout the paper, let

$$P_k(\mathcal{T}) = \{v_k : \Omega \to \mathbb{R} \mid \forall T \in \mathcal{T}, v_k|_T \text{ is a polynomial of total degree} \leq k\}$$

denote the set of piecewise polynomials and $\Pi_0 : L^2(\Omega) \to P_0(\mathcal{T})$ denote the L^2-projection onto $\mathcal{T}$-piecewise constant functions or vectors, i.e., $(\Pi_0 f)|_T = \fint_T f \,\mathrm{d}x$ for all $T \in \mathcal{T}$ and all $f \in L^2(\Omega;\mathbb{R}^m)$.

Given such a shape-regular triangulation $\mathcal{T}$, recall the three FEM under consideration.

CFEM. The Courant finite element space reads

$$V_{\mathrm{C}}(\mathcal{T}) := \{v_{\mathrm{C}} \in P_1(\mathcal{T}) \mid v_{\mathrm{C}} \text{ is continuous and vanishes on } \partial\Omega\}. \tag{2.1.a}$$

The corresponding (unique) Galerkin approximation $u_{\mathrm{C}} \in V_{\mathrm{C}}(\mathcal{T})$ satisfies

$$\int_\Omega \nabla u_{\mathrm{C}} \cdot \nabla v_{\mathrm{C}} \,\mathrm{d}x = \int_\Omega f v_{\mathrm{C}} \,\mathrm{d}x \quad \text{for all } v_{\mathrm{C}} \in V_{\mathrm{C}}(\mathcal{T}). \tag{2.1.b}$$

CR-NCFEM. The Crouzeix-Raviart finite element space reads

$$\mathrm{CR}^1_0(\mathcal{T}) := \{v_{\mathrm{CR}} \in P_1(\mathcal{T}) \mid v_{\mathrm{CR}} \text{ is continuous at midpoints of interior edges and vanishes at midpoints of boundary edges}\}. \quad (2.2.a)$$

A general function in $\mathrm{CR}^1_0(\mathcal{T})$ does not belong to $H^1(\Omega)$. However, the $\mathcal{T}$-piecewise gradient $\nabla_{\mathrm{NC}} v_{\mathrm{CR}}$, with $(\nabla_{\mathrm{NC}} v_{\mathrm{CR}})|_T = \nabla(v_{\mathrm{CR}}|_T)$ for all $T \in \mathcal{T}$, exists and $\nabla_{\mathrm{NC}} v_{\mathrm{CR}} \in P_0(\mathcal{T}; \mathbb{R}^2)$. The (unique) Crouzeix-Raviart approximation $u_{\mathrm{CR}} \in \mathrm{CR}^1_0(\mathcal{T})$ satisfies

$$\int_\Omega \nabla_{\mathrm{NC}} u_{\mathrm{CR}} \cdot \nabla_{\mathrm{NC}} v_{\mathrm{CR}} \,\mathrm{d}x = \int_\Omega f v_{\mathrm{CR}} \,\mathrm{d}x \quad \text{for all } v_{\mathrm{CR}} \in \mathrm{CR}^1_0(\mathcal{T}). \quad (2.2.b)$$

RT-MFEM. The mixed lowest-order Raviart-Thomas finite element space reads

$$\mathrm{RT}_0(\mathcal{T}) := \{q \in H(\mathrm{div}, \Omega) \mid \forall T \in \mathcal{T}\, \exists\, a_T \in \mathbb{R}^2\, \exists\, b_T \in \mathbb{R}\, \forall x \in T,\ q|_T(x) = a_T + b_T x\}. \quad (2.3.a)$$

The (unique) mixed finite element approximation $(p_{\mathrm{RT}}, u_{\mathrm{RT}}) \in \mathrm{RT}_0(\mathcal{T}) \times P_0(\mathcal{T})$ satisfies

$$\begin{aligned} \int_\Omega p_{\mathrm{RT}} \cdot q_{\mathrm{RT}} \,\mathrm{d}x + \int_\Omega u_{\mathrm{RT}} \,\mathrm{div}\, q_{\mathrm{RT}} \,\mathrm{d}x &= 0 \qquad \text{for all } q_{\mathrm{RT}} \in \mathrm{RT}_0(\mathcal{T}); \\ \Pi_0 f + \mathrm{div}\, p_{\mathrm{RT}} &= 0. \end{aligned} \quad (2.3.b)$$

2.2 Main Results

This subsection presents the comparison results proved in Section 3. The Lebesgue and Sobolev spaces $L^2(\Omega)$ and $H^1(\Omega)$ are defined as usual, $\mathrm{C}(\Omega)$ denotes the set of continuous functions on Ω and we define $\|\cdot\| := \|\cdot\|_{L^2(\Omega)}$ and $\mathrm{osc}(f, \mathcal{T}) := \|h_{\mathcal{T}}(f - \Pi_0 f)\|$.

Theorem 1 (Equivalence of CFEM and CR-NCFEM). *It holds*

$$\|\nabla u - \nabla u_{\mathrm{C}}\| \lesssim \|\nabla u - \nabla_{\mathrm{NC}} u_{\mathrm{CR}}\| \lesssim \|\nabla u - \nabla u_{\mathrm{C}}\| + \mathrm{osc}(f, \mathcal{T}).$$

Theorem 2 (Comparison of RT-MFEM and CR-NCFEM). *It holds*

$$\|\nabla u - \nabla_{\mathrm{NC}} u_{\mathrm{CR}}\| \lesssim \|hf\| + \|\nabla u - p_{\mathrm{RT}}\| \lesssim \|\nabla u - \nabla_{\mathrm{NC}} u_{\mathrm{CR}}\| + \mathrm{osc}(f, \mathcal{T}).$$

Theorem 3 (Superiority of RT-MFEM). *The conjecture*

$$\|\nabla u - \nabla_{\mathrm{NC}} u_{\mathrm{CR}}\| \lesssim \|\nabla u - p_{\mathrm{RT}}\| + \mathrm{osc}(f, \mathcal{T})$$

is false in general in the sense that, given $f \equiv 2$ and $M > 0$, there exist some convex Lipschitz domain $\Omega = \Omega_M$ and a quasi uniform triangulation $\mathcal{T} = \mathcal{T}_M$ such that

$$M\left(\|\nabla u - p_{\mathrm{RT}}\| + \mathrm{osc}(f, \mathcal{T})\right) \le \|\nabla u - \nabla_{\mathrm{NC}} u_{\mathrm{CR}}\|.$$

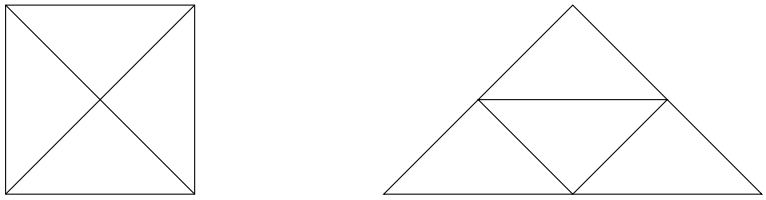

Figure 2.1: Criss-cross triangulation of the unit square (left) and a red-refined triangle (right).

2.3 Comments

Two possible conjectures. In the context of Theorems 1–3 and the hypercircle identities, two possible conjectures read

$$\|\nabla u - \nabla u_{\mathrm{C}}\| \lesssim \|\nabla u_{\mathrm{C}} - \nabla_{\mathrm{NC}} u_{\mathrm{CR}}\| + \operatorname{osc}(f, \mathcal{T})$$

and

$$\|\nabla u - \nabla_{\mathrm{NC}} u_{\mathrm{CR}}\| \lesssim \|\nabla u_{\mathrm{C}} - \nabla_{\mathrm{NC}} u_{\mathrm{CR}}\| + \operatorname{osc}(f, \mathcal{T}).$$

The two statements are false in general, because for $f \equiv 1$, and the criss-cross triangulation $\mathcal{T}$ of the unit square $\Omega = [0,1]^2$ into four congruent triangles as depicted in Figure 2.1, it holds $u_{\mathrm{C}} = u_{\mathrm{CR}} \neq u$.

Results for the Least-Squares FEM. Amongst the possible immediate applications, we briefly discuss the least-squares finite element method. The least-squares functional

$$\mathrm{LS}(f; q_{\mathrm{LS}}, v_{\mathrm{LS}}) := \|f + \operatorname{div} q_{\mathrm{LS}}\|^2 + \|q_{\mathrm{LS}} - \nabla v_{\mathrm{LS}}\|^2$$

is minimised amongst all $(q_{\mathrm{LS}}, v_{\mathrm{LS}}) \in \mathrm{RT}_0(\mathcal{T}) \times V_{\mathrm{C}}(\mathcal{T})$. It is well known [3] that the Least-Squares FEM is quasi-optimal in the sense that

$$\|\nabla u - p_{\mathrm{LS}}\|_{H(\operatorname{div},\Omega)} + \|\nabla(u - u_{\mathrm{LS}})\| \lesssim \min_{q_{\mathrm{RT}} \in \mathrm{RT}_0(\mathcal{T})} \|\nabla u - q_{\mathrm{RT}}\|_{H(\operatorname{div},\Omega)} + \min_{v_{\mathrm{C}} \in V_{\mathrm{C}}(\mathcal{T})} \|\nabla(u - v_{\mathrm{C}})\|.$$

In particular, with regard to Theorems 1 and 2, the choice $q_{\mathrm{RT}} := p_{\mathrm{RT}}$ and $v_{\mathrm{C}} := u_{\mathrm{C}}$ for p_{RT} and u_{C} the Raviart-Thomas and the Courant solution leads to

$$\|\nabla u - p_{\mathrm{LS}}\|_{H(\operatorname{div},\Omega)} + \|\nabla(u - u_{\mathrm{LS}})\| \approx \|\nabla(u - u_{\mathrm{C}})\| + \|f - \Pi_0 f\|. \tag{2.4}$$

Since $\|\nabla(u - u_{\mathrm{C}})\| \leq \|\nabla(u - u_{\mathrm{LS}})\|$, this proves

$$\|\nabla u - p_{\mathrm{LS}}\|_{H(\operatorname{div},\Omega)} \lesssim \|\nabla(u - u_{\mathrm{LS}})\| + \|f - \Pi_0 f\|.$$

The counterexample from Theorem 3 shows that the possible conjecture

$$\|\nabla(u - u_{\mathrm{LS}})\| \lesssim \|\nabla u - p_{\mathrm{LS}}\| + \|f - \Pi_0 f\|$$

is false in general. This is a consequence of supercloseness of [6] and elementary calculations. This result is counterintuitive in the sense that the rule of thumb in minimisation of $\mathrm{LS}(f; \bullet, \bullet)$ expects two contributions of similar size.

At least for piecewise constant right-hand sides f, the equivalence (2.4) is also an improvement of [15, Theorem 5.1] on the separate approximation within the least-squares method.

Equality of Approximation Classes. The notion of optimality of adaptive FEM in the literature is based on the concept of an approximation class [9, 2]. Given some $s > 0$ and an initial regular triangulation $\mathcal{T}_0$, one defines admissible triangulations $\mathcal{T}$ with $|\mathcal{T}| \leq |\mathcal{T}_0| + N$ and considers a minimum of an approximation term $\mathrm{approx}(\mathcal{T}, u, f)$ specified below. For the Courant FEM,

$$\mathrm{approx}(\mathcal{T}, u, f) := \sqrt{\|\nabla u - \nabla u_{\mathrm{C}}\|^2 + \mathrm{osc}(f, \mathcal{T})^2},$$

where $u_{\mathrm{C}} \in V_{\mathrm{C}}(\mathcal{T})$ is the solution of (2.1.b) with right-hand side f. For CR-NCFEM [1, 17],

$$\mathrm{approx}(\mathcal{T}, u, f) := \sqrt{\|\nabla u - \nabla_{\mathrm{NC}} u_{\mathrm{CR}}\|^2 + \|h_{\mathcal{T}} f\|^2}$$

or (the equivalent term)

$$\mathrm{approx}(\mathcal{T}, u, f) := \sqrt{\|\nabla u - \nabla_{\mathrm{NC}} u_{\mathrm{CR}}\|^2 + \mathrm{osc}(f, \mathcal{T})^2}$$

are in use for the CR-NCFEM solution $u_{\mathrm{CR}} \in \mathrm{CR}^1_0(\mathcal{T})$ of (2.2.b) with right-hand side f. For RT-MFEM [8, Definition 3.5], [10],

$$\mathrm{approx}(\mathcal{T}, u, f) := \sqrt{\|\nabla u - p_{\mathrm{RT}}\|^2 + \mathrm{osc}(f, \mathcal{T})^2}$$

are in use for the discrete solution $p_{\mathrm{RT}} \in \mathrm{RT}_0(\mathcal{T})$ based on (2.3) with data f.

Given any such approximation term $\mathrm{approx}(\mathcal{T}, u, f)$, the approximation class

$$\mathcal{A}_s := \{(u, f) \in H^1_0(\Omega) \times L^2(\Omega) \mid u \text{ solves (1.1) with right-hand side } f \text{ and } |(u, f)|_{\mathcal{A}_s} < \infty\}$$

is defined via the seminorm

$$|(u, f)|_{\mathcal{A}_s} := \sup_{N \in \mathbb{N}} \min_{|\mathcal{T}| \leq N + |\mathcal{T}_0|} N^s \, \mathrm{approx}(\mathcal{T}, u, f).$$

Clearly, the approximation class depends on the approximation term $\mathrm{approx}(\mathcal{T}, u, f)$ at hand and hence on the FEM at hand. Correspondingly, we have

$$\mathcal{A}_s(\mathrm{C}), \mathcal{A}_s(\mathrm{CR}), \text{ and } \mathcal{A}_s(\mathrm{RT})$$

according to the above choices related to the discretisation scheme at hand. From the comparison results of this paper, we deduce

$$\mathcal{A}_s := \mathcal{A}_s(\mathrm{C}) = \mathcal{A}_s(\mathrm{CR}) \subset \mathcal{A}_s(\mathrm{RT})$$

for $\mathcal{A}_s$ defined as before with $p := \nabla u$ and the approximation term

$$\mathrm{approx}(\mathcal{T}, u, f) := \sqrt{\|p - \Pi_0 p\|^2 + \mathrm{osc}(f, \mathcal{T})^2}.$$

The aforementioned result (1.3) from [14, Section 3.1] leads to

$$\|p - \Pi_0 p\| + \mathrm{osc}(f, \mathcal{T}) \approx \|\nabla u - \nabla_{\mathrm{NC}} u_{\mathrm{CR}}\| + \mathrm{osc}(f, \mathcal{T})$$

and, hence, (1.2) proves the equivalence of the approximation terms which then shows the equality of the approximation classes.

The counterexample of Theorem 3 motivates the conjecture

$$\mathcal{A}_s(\mathrm{RT}) \neq \mathcal{A}_s.$$

A detailed discussion of a proof requires the approximation of the curved boundary $\partial B(0, 1)$ (it is no longer sufficient to consider refinements of some fixed $\mathcal{T}_0$) and lies beyond the scope of this paper. Similar arguments apply to the approximation classes of the least square finite element method.

3 Proofs

3.1 Proof of Theorem 1

The first proposition is already included in [7, Theorem 5.1] with a different proof.

Proposition 4. *Any* $v_{\mathrm{CR}} \in \mathrm{CR}^1_0(\mathcal{T})$ *satisfies*

$$\min_{v_{\mathrm{C}} \in V_{\mathrm{C}}(\mathcal{T})} \|\nabla_{\mathrm{NC}} v_{\mathrm{CR}} - \nabla v_{\mathrm{C}}\| \approx \min_{v \in H^1_0(\Omega)} \|\nabla_{\mathrm{NC}} v_{\mathrm{CR}} - \nabla v\|.$$

Proof. Let $\Omega_T := \cup\{K \in \mathcal{T} \mid T \cap K \neq \emptyset\}$ denote the patch of first order layers around T and let $\mathcal{E}(\Omega_T) := \{E \in \mathcal{E} \mid E \cap T \neq \emptyset\}$ and $\mathcal{T}(\Omega_T) := \{T \in \mathcal{T} \mid T \subset \Omega_T\}$ denote its edges and triangles. For $z \in \mathcal{N}$ define $\mathcal{T}(z) := \{T \in \mathcal{T} \mid z \in T\}$.

Given $v_{\mathrm{CR}} \in \mathrm{CR}^1_0(\mathcal{T})$ define $\mathrm{I_C}\, v_{\mathrm{CR}} \in V_{\mathrm{C}}(\mathcal{T})$ by

$$(\mathrm{I_C}\, v_{\mathrm{CR}})(z) = |\mathcal{T}(z)|^{-1} \sum_{T \in \mathcal{T}(z)} (v_{\mathrm{CR}}|_T)(z) \tag{3.1}$$

for any interior node $z \in \mathcal{N}(\Omega)$. For $v_{\mathrm{CR}} \in \mathrm{CR}^1_0(\mathcal{T}(\Omega_T))$, define

$$\rho_1(v_{\mathrm{CR}}) := \|\nabla_{\mathrm{NC}}(v_{\mathrm{CR}} - \mathrm{I_C}\, v_{\mathrm{CR}})\|_{L^2(T)}$$

and

$$\rho_2(v_{\mathrm{CR}}) := \sqrt{\sum_{E \in \mathcal{E}(\Omega_T)} |E| \|[(\nabla_{\mathrm{NC}} v_{\mathrm{CR}}) \cdot \tau_E]_E\|^2_{L^2(E)}}\,,$$

where τ_E denotes a unit vector tangential to E. If $\rho_2(v_{\mathrm{CR}}) = 0$, then $v_{\mathrm{CR}} \in \mathrm{C}(\Omega_T)$ and $v_{\mathrm{CR}}|_E = 0$ for a boundary edge $E \subset \partial\Omega \cap \bar{\Omega}_T$, hence $\mathrm{I_C}\, v_{\mathrm{CR}} = v_{\mathrm{CR}}$ on T and $\rho_1(v_{\mathrm{CR}}) = 0$. Since ρ_1 and ρ_2 are seminorms on $\mathrm{CR}^1_0(\mathcal{T}(\Omega_T))$, there exists a constant, such that $\rho_1 \lesssim \rho_2$ on $\mathrm{CR}^1_0(\mathcal{T}(\Omega_T))$. A scaling argument shows that the constant is independent of the mesh-size. The sum over all $T \in \mathcal{T}$ and the bounded overlap of the patches $(\Omega_T \mid T \in \mathcal{T})$ show that

$$\|\nabla_{\mathrm{NC}}(v_{\mathrm{CR}} - \mathrm{I_C}\, v_{\mathrm{CR}})\| \lesssim \sqrt{\sum_{E \in \mathcal{E}} |E| \, \|[(\nabla_{\mathrm{NC}} v_{\mathrm{CR}}) \cdot \tau_E]_E\|^2_{L^2(E)}}\,.$$

By a straight-forward modification of [13, Theorem 3.1],

$$\sqrt{\sum_{E \in \mathcal{E}} |E| \, \|[(\nabla_{\mathrm{NC}} v_{\mathrm{CR}}) \cdot \tau_E]_E\|^2_{L^2(E)}} \approx \min_{v \in H^1_0(\Omega)} \|\nabla_{\mathrm{NC}} v_{\mathrm{CR}} - \nabla v\|\,.$$

Hence, one inequality is proven. The reverse inequality follows from $\nabla V_{\mathrm{C}}(\mathcal{T}) \subset \nabla H^1_0(\Omega)$. ∎

The remaining part of this subsection is devoted to our proof of Theorem 1. A different proof can be found in [5]. The inclusion $V_{\mathrm{C}}(\mathcal{T}) \subset \mathrm{CR}^1_0(\mathcal{T})$ and Galerkin orthogonality show

$$\|\nabla_{\mathrm{NC}} u_{\mathrm{CR}} - \nabla u_{\mathrm{C}}\| = \min_{v_{\mathrm{C}} \in V_{\mathrm{C}}(\mathcal{T})} \|\nabla_{\mathrm{NC}} u_{\mathrm{CR}} - \nabla v_{\mathrm{C}}\|\,.$$

Together with Proposition 4 and the triangle inequality it follows

$$\|\nabla u - \nabla u_{\mathrm{C}}\| \le \|\nabla u - \nabla_{\mathrm{NC}} u_{\mathrm{CR}}\| + \|\nabla_{\mathrm{NC}} u_{\mathrm{CR}} - \nabla u_{\mathrm{C}}\| \lesssim \|\nabla u - \nabla_{\mathrm{NC}} u_{\mathrm{CR}}\|$$

which is the first inequality in Theorem 1.

For the proof of the second inequality let $e := \mathrm{I}_{\mathrm{NC}}\, u - u_{\mathrm{CR}}$, where the nonconforming interpolation $\mathrm{I}_{\mathrm{NC}}\, u \in \mathrm{CR}^1_0(\mathcal{T})$ is defined uniquely by

$$\fint_E \mathrm{I}_{\mathrm{NC}}\, u \,\mathrm{d}s = \fint_E u \,\mathrm{d}s \quad \text{for all } E \in \mathcal{E}.$$

Since $\nabla_{\mathrm{NC}}(\mathrm{I}_{\mathrm{NC}}\, u) = \Pi_0(\nabla u)$, it holds

$$\begin{aligned} \|\nabla u - \nabla_{\mathrm{NC}} u_{\mathrm{CR}}\|_{L^2(\Omega)} &\le \|\nabla u - \nabla_{\mathrm{NC}}\, \mathrm{I}_{\mathrm{NC}}\, u\|_{L^2(\Omega)} + \|\nabla_{\mathrm{NC}} e\|_{L^2(\Omega)} \\ &\le \|\nabla(u - u_{\mathrm{C}})\|_{L^2(\Omega)} + \|\nabla_{\mathrm{NC}} e\|_{L^2(\Omega)}. \end{aligned} \tag{3.2}$$

Since $\nabla_{\mathrm{NC}} e$ is constant on $E \in \mathcal{E}$, $[e]$ is affine on $E \in \mathcal{E}$ and vanishes in the midpoint of E, it follows for $e_{\mathrm{C}} := \mathrm{I}_{\mathrm{C}}\, e \in V_{\mathrm{C}}(\mathcal{T})$ (with I_{C} from (3.1)) that

$$\begin{aligned} \|\nabla_{\mathrm{NC}} e\|^2_{L^2(\Omega)} &= \int_\Omega \nabla_{\mathrm{NC}} e \cdot \nabla_{\mathrm{NC}}(e - e_{\mathrm{C}}) \,\mathrm{d}x \\ &= \sum_{E\in\mathcal{E}} \int_E [(e - e_{\mathrm{C}}) \nabla_{\mathrm{NC}} e \cdot \nu_E]_E \,\mathrm{d}s \\ &\le \sum_{E\in\mathcal{E}:E\subset\Omega} \|[\nabla_{\mathrm{NC}} e \cdot \nu_E]_E\|_{L^2(E)} \left\|\langle e - e_{\mathrm{C}}\rangle_E\right\|_{L^2(E)} \\ &\le \sqrt{\sum_{E\in\mathcal{E}:E\subset\Omega} |E| \,\|[\nabla_{\mathrm{NC}} e \cdot \nu_E]_E\|^2_{L^2(E)}} \sqrt{\sum_{E\in\mathcal{E}} |E|^{-1} \left\|\langle e - e_{\mathrm{C}}\rangle_E\right\|^2_{L^2(E)}}. \end{aligned}$$

Let $\Omega_E := \cup\{T \in \mathcal{T} \mid E \cap T \neq \emptyset\}$ denote the patch of first order around E and let $\mathcal{T}(\Omega_E)$ denote its triangles. Define for $v_{\mathrm{CR}} \in \mathrm{CR}^1(\mathcal{T}(\Omega_E))$

$$\rho_3(v_{\mathrm{CR}}) := |E|^{-\frac{1}{2}} \left\|\langle v_{\mathrm{CR}} - \mathrm{I}_{\mathrm{C}}\, v_{\mathrm{CR}}\rangle_E\right\|_{L^2(E)} \text{ and } \rho_4(v_{\mathrm{CR}}) := \|\nabla_{\mathrm{NC}} v_{\mathrm{CR}}\|_{L^2(\Omega_E)}.$$

If $\rho_4(v_{\mathrm{CR}}) = 0$ then v_{CR} is constant on each $T \in \mathcal{T}(\Omega_E)$. Since v_{CR} is continuous on the midpoints of interior edges of $\mathcal{T}(\Omega_E)$, v_{CR} is constant on Ω_E. Hence, $v_{\mathrm{CR}} = \mathrm{I}_{\mathrm{C}}\, v_{\mathrm{CR}}$ on E and $\rho_3(v_{\mathrm{CR}}) = 0$. Since ρ_3 and ρ_4 are seminorms on $\mathrm{CR}^1(\mathcal{T}(\Omega_E))$, there exists a constant such that $\rho_3 \lesssim \rho_4$ on $\mathrm{CR}^1(\mathcal{T}(\Omega_E))$. A scaling argument shows that the constant is independent of the mesh-size. The sum over all interior edges of $\mathcal{T}$ and the bounded overlap of the patches $(\Omega_E \mid E \in \mathcal{E})$ show that

$$\sum_{E\in\mathcal{E}} |E|^{-1} \left\|\langle e - e_{\mathrm{C}}\rangle_E\right\|^2_{L^2(E)} \lesssim \|\nabla_{\mathrm{NC}} e\|^2.$$

This leads to

$$\|\nabla_{\mathrm{NC}} e\|^2 \lesssim \sum_{E\in\mathcal{E}} |E| \,\|[\nabla_{\mathrm{NC}} e \cdot \nu_E]_E\|^2_{L^2(E)}\,. \tag{3.3}$$

For any vertex $x \in \mathcal{N}$ let φ_x denote the associated hat function (i.e., φ_x is continuous, $\mathcal{T}$-piecewise affine, and $\varphi_x(y) = \delta_{xy}$ for all $y \in \mathcal{N}$). Given any $E =$

$\mathrm{conv}\{a,b\} \in \mathcal{E}$ with $E = T_+ \cap T_-$ for $T_+ = \mathrm{conv}\{a,b,c\}, T_- = \mathrm{conv}\{a,b,d\} \in \mathcal{T}$, let $b_E := 6\,\varphi_a\varphi_b - 10\varphi_a\varphi_b\varphi_c - 10\varphi_a\varphi_b\varphi_d$ be some bubble function supported on $\omega_E := T_+ \cup T_-$. Compute

$$\begin{aligned}
|E|^{1/2}\,\|[(\nabla_{\mathrm{NC}} e)\cdot\nu_E]_E\|_{L^2(E)} &= \left|\int_E [(\nabla_{\mathrm{NC}}\,\mathrm{I}_{\mathrm{NC}}\,u - \nabla_{\mathrm{NC}} u_{\mathrm{CR}})\cdot\nu_E]_E\,\mathrm{d}s\right| \\
&= \left|\int_E b_E\,[(\nabla_{\mathrm{NC}}\,\mathrm{I}_{\mathrm{NC}}\,u - u)\cdot\nu_E]_E\,\mathrm{d}s - \int_E \psi_E\,[(\nabla_{\mathrm{NC}} u_{\mathrm{CR}})\cdot\nu_E]_E\,\mathrm{d}s\right| \\
&= \left|\int_{\omega_E} \nabla_{\mathrm{NC}}(\mathrm{I}_{\mathrm{NC}}\,u - u)\cdot\nabla b_E\,\mathrm{d}x - \int_\Omega \Delta u\; b_E\,\mathrm{d}x - \int_\Omega \nabla_{\mathrm{NC}} u_{\mathrm{CR}}\cdot\nabla_{\mathrm{NC}}\psi_E\,\mathrm{d}x\right| \\
&\le \left|\int_\Omega \nabla_{\mathrm{NC}}(\mathrm{I}_{\mathrm{NC}}\,u - u)\cdot\nabla b_E\,\mathrm{d}x\right| + \left|\int_\Omega f(b_E - \psi_E)\,\mathrm{d}x\right|.
\end{aligned} \tag{3.4}$$

Since, by definition, $\fint_{T_\pm}(b_E - \psi_E)\,\mathrm{d}x = 0$ and $\|b_E - \psi_E\|_{L^\infty(\Omega)} \approx 1$, the Poincaré inequality leads to

$$\left|\int_\Omega f(b_E - \psi_E)\,\mathrm{d}x\right| = \left|\int_{\omega_E} (f - \Pi_0 f)\,(b_E - \psi_E)\,\mathrm{d}x\right| \lesssim |\omega_E|^{1/2}\|f - \Pi_0 f\|_{L^2(\omega_E)}. \tag{3.5}$$

Moreover, $\|\nabla b_E\|_{L^2(\Omega)} \approx 1$ and $\nabla_{\mathrm{NC}}\,\mathrm{I}_{\mathrm{NC}}\,u = \Pi_0(\nabla u)$ yield

$$\left|\int_\Omega \nabla_{\mathrm{NC}}(\mathrm{I}_{\mathrm{NC}}\,u - u)\cdot\nabla b_E\,\mathrm{d}x\right| \lesssim \|\nabla_{\mathrm{NC}}(u - \mathrm{I}_{\mathrm{NC}}\,u)\|_{L^2(\omega_E)} \le \|\nabla(u - u_{\mathrm{C}})\|_{L^2(\omega_E)}. \tag{3.6}$$

The combination of (3.2)–(3.6) plus the finite overlap of $(\omega_E \mid E \in \mathcal{E})$ proves the second inequality in Theorem 1.

3.2 Proof of Theorem 2

Let $\tilde{u}_{\mathrm{CR}} \in \mathrm{CR}^1_0(\mathcal{T})$ denote the Crouzeix-Raviart solution with respect to the right-hand side $f = \Pi_0 f$. Marini [16] shows that

$$p_{\mathrm{RT}} = \nabla_{\mathrm{NC}}\tilde{u}_{\mathrm{CR}} - \tfrac{1}{2}(\Pi_0 f)(\bullet - \mathrm{mid}(\mathcal{T}))$$

where $\mathrm{mid}(\mathcal{T})|_T = \mathrm{mid}(T)$ and $\mathrm{mid}(T)$ denotes the barycentre of $T \in \mathcal{T}$ and $(\bullet - \mathrm{mid}(T)) \in P_1(\mathcal{T})$ equals $(x - \mathrm{mid}(T))$ at $x \in T \in \mathcal{T}$. Hence,

$$\begin{aligned}
\|\nabla u - \nabla_{\mathrm{NC}} u_{\mathrm{CR}}\| &\le \|\nabla u - p_{\mathrm{RT}}\| + \|p_{\mathrm{RT}} - \nabla_{\mathrm{NC}}\tilde{u}_{\mathrm{CR}}\| + \|\nabla_{\mathrm{NC}}\tilde{u}_{\mathrm{CR}} - \nabla_{\mathrm{NC}} u_{\mathrm{CR}}\| \\
&\lesssim \|\nabla u - p_{\mathrm{RT}}\| + \|hf\|.
\end{aligned}$$

This proves the first inequality in Theorem 2. The proof of the second one exploits Marini's identity again,

$$\|\nabla u - p_{\mathrm{RT}}\| \le \|\nabla u - \nabla_{\mathrm{NC}}\tilde{u}_{\mathrm{CR}}\| + \|\nabla_{\mathrm{NC}}\tilde{u}_{\mathrm{CR}} - p_{\mathrm{RT}}\| \lesssim \|\nabla u - \nabla_{\mathrm{NC}} u_{\mathrm{CR}}\| + \|hf\|.$$

The efficiency of $\|hf\|$ up to oscillations [19], namely

$$\|hf\| \lesssim \|\nabla u - \nabla_{\mathrm{NC}} u_{\mathrm{CR}}\| + \operatorname{osc}(f), \tag{3.7}$$

concludes the proof.

3.3 Proof of Theorem 3

The counterexample concerns the quadratic polynomial u_B,

$$u_B(x) := (1 - |x|^2)/2 \quad \text{in the unit disk } B = B(0,1).$$

Note that $u_B \in C^\infty(\mathbb{R}^2)$ solves $-\Delta u = 2$ in B and $u = 0$ on ∂B. Moreover, $\nabla u = -x \in \mathrm{RT}_0(\mathcal{T})$.

Given a small $0 < h \ll 1$ as the uniform edge-length of a regular polygon Ω with vertices on ∂B, let $\mathcal{T}$ denote a shape-regular quasi-uniform triangulation of Ω with maximal mesh size $\approx h$. Let $u \in H^1_0(\Omega)$ solve $-\Delta u = 2$ in Ω.

The point of departure is the claim $\|\nabla(u - u_B)\| \lesssim h^{3/2}$. To prove this, observe that, since $u_B - u$ is harmonic with boundary values $u_B|_{\partial\Omega}$,

$$\|\nabla(u - u_B)\| = \min\{\, \|\nabla v\| \mid v \in H^1(\Omega) :\ v|_{\partial\Omega} = u_B|_{\partial\Omega}\}.$$

Therefore it remains to design some function $w \in H^1(\Omega)$ with $w|_{\partial\Omega} = u_B|_{\partial\Omega}$ and $\|\nabla w\| \lesssim h^{3/2}$. To do so, set for any $E \in \mathcal{E}$ with $E = \operatorname{conv}\{a,b\} = \partial\Omega \cap T$ for some $T \in \mathcal{T}$ and nodal basis functions φ_a and φ_b of the Courant FEM,

$$w_E := \frac{1}{2} h^2 \varphi_a \varphi_b \in H^1(\Omega) \ \text{ with } \ \operatorname{supp} w_E = T \quad \text{and} \quad w = \left(\sum_{E \in \mathcal{E}: E \subset \partial\Omega} w_E \right) \in H^1(\Omega).$$

Since $w_E(x) = u_B(x)$ for all $x \in E$, and $\|\nabla w_E\| \approx h^2$, it follows

$$\|\nabla(u - u_B)\| \leq \sqrt{\sum_{E \in \mathcal{E}: E \subset \partial\Omega} \|\nabla w_E\|^2} \approx h^{3/2}.$$

For $Q(f, \mathcal{T}) := \{q_{\mathrm{RT}} \in \mathrm{RT}_0(\mathcal{T}) \mid \operatorname{div} q_{\mathrm{RT}} = -\Pi_0 f\}$, the RT-MFEM approximation p_{RT} of ∇u on Ω is characterised by

$$\|\nabla u - p_{\mathrm{RT}}\| = \min\{\, \|\nabla u - q_{\mathrm{RT}}\| \mid q_{\mathrm{RT}} \in Q(2, \mathcal{T})\}.$$

This is well-understood in the context of minimisation under side restrictions and its connection to saddle-point problems [4]. Since $\nabla u_B \in Q(2, \mathcal{T})$, it follows

$$\|\nabla u - p_{\mathrm{RT}}\| \leq \|\nabla(u - u_B)\| \lesssim h^{3/2}. \tag{3.8}$$

Since $f \equiv 2$, it holds $\operatorname{osc} f = 0$ and $\|hf\| \approx h$. Hence, (3.7) and (3.8) imply

$$Ch^{-1/2}(\|\nabla u - p_{\mathrm{RT}}\| + \operatorname{osc}(f, \mathcal{T})) \leq \|\nabla u - \nabla_{\mathrm{NC}} u_{\mathrm{CR}}\|$$

Given $M > 0$, the choice $h = (C/M)^2$ proves the assertion of Theorem 3.

4 Numerical Illustration

The first experiment illustrates the counterexample of Theorem 3 which appears to be non-generic. The second example with a corner-singularity shows equality of convergence rates as a typical behaviour.

4.1 Illustration of Theorem 3

In the first experiment, the domains Ω_j, $j = 2, 3, \ldots, 9$, are regular polygons with 2^j edges whose vertices lie on the unit sphere $\partial B(0, 1)$ as in the proof of Theorem 3. For each domain Ω_j a series of red-refined triangulations $\mathcal{T}_{j,\ell} := \mathrm{red}^{(\ell)}(\mathcal{T}_j)$ of an initial triangulation $\mathcal{T}_j$ determines the discrete solutions $u_{\mathrm{CR}}^{(j,\ell)}$ and $p_{\mathrm{RT}}^{(j,\ell)}$ of (2.2.b) and (2.3.b). For the red-refinement of the triangulation each triangle is refined as in Figure 2.1. The initial triangulations are given as follows. $\mathcal{T}_2$ is the criss-cross triangulation and given the triangulation $\mathcal{T}_j$, a red-refinement $\mathrm{red}(\mathcal{T}_j)$ of $\mathcal{T}_j$ is modified in that the new boundary nodes are projected to the circle $\partial B(0, 1)$. This defines $\mathcal{T}_{j+1}$; the triangulations $\mathcal{T}_2$, $\mathcal{T}_3$, $\mathcal{T}_6$ are depicted in Figure 4.1.

Table 1 contains the quotients of the flux errors with exact solution $u^{(j)}$ based on the Poisson model problem on Ω_j and its flux approximations $\nabla_{\mathrm{NC}} u_{\mathrm{CR}}^{(j,\ell)}$ and $p_{\mathrm{RT}}^{(j,\ell)}$ based on the triangulation $\mathcal{T}_{j,\ell}$,

$$q(\ell, j) := \frac{\|\nabla u^{(j)} - p_{\mathrm{RT}}^{(j,\ell)}\|}{\|\nabla u^{(j)} - \nabla_{\mathrm{NC}} u_{\mathrm{CR}}^{(j,\ell)}\|}. \tag{4.1}$$

The convergence history plot of Figure 4.2 shows the flux errors plotted against the number of degrees of freedom. The crosses and the triangles mark the errors for the Crouzeix-Raviart and the Raviart-Thomas solution. In order to compute the error, for each domain Ω_j some P_2 reference solution is computed on $\mathcal{T}_{j,11-j}$. The dashed lines connect the errors for the triangulations $\mathcal{T}_2, \mathcal{T}_3, \ldots, \mathcal{T}_9$ of the proof of Theorem 3 and show the expected convergence rates.

The Raviart-Thomas errors show a larger convergence rate on the initial triangulations than the Crouzeix-Raviart errors, while for a fixed domain the Raviart-Thomas errors converge with the same convergence rate as the Crouzeix-Raviart errors after a very long preasymptotic plateaux. The same behaviour can be observed in Table 1: For a fixed ℓ the quotients $q(\ell, j)$ are decreasing while for a fixed j the quotients first increase and then stay on the same level.

4.2 Numerical Comparison on L-shaped Domain

The second example is devoted to a prototypical equivalent behaviour of the three finite element schemes. The corner singular functions on a typical corner of a

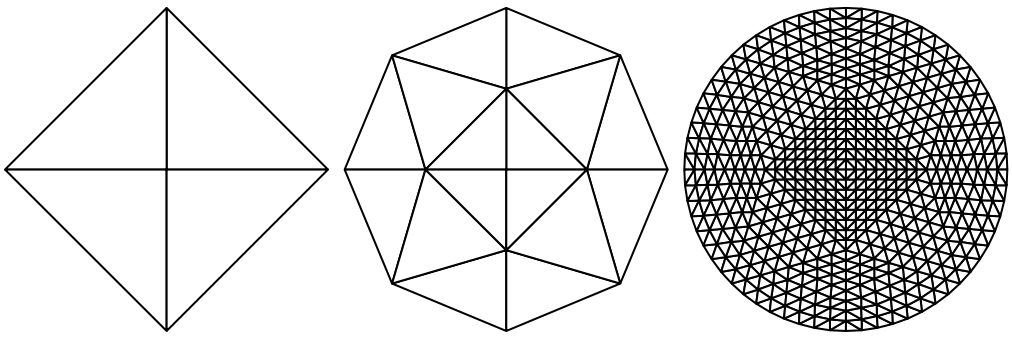

Figure 4.1: $\mathcal{T}_2$, $\mathcal{T}_3$ and $\mathcal{T}_6$ from Subsection 4.1

Table 1: Quotient $q(\ell, j)$ from (4.1) for RT-MFEM and CR-NCFEM

	$\ell = 0$	1	2	3	4	5	6	7
$j = 2$	.94097	.90727	.90405	.90346	.90335	.90333	.90333	.90333
3	.51218	.72172	.77759	.80313	.81703	.82517	.83011	
4	.34413	.56908	.66257	.71381	.74579	.76746		
5	.23909	.43216	.53576	.60128	.64662			
6	.16793	.31867	.41264	.47906				
7	.11856	.23084	.30735					
8	.08424	.16622						
9	.06103							

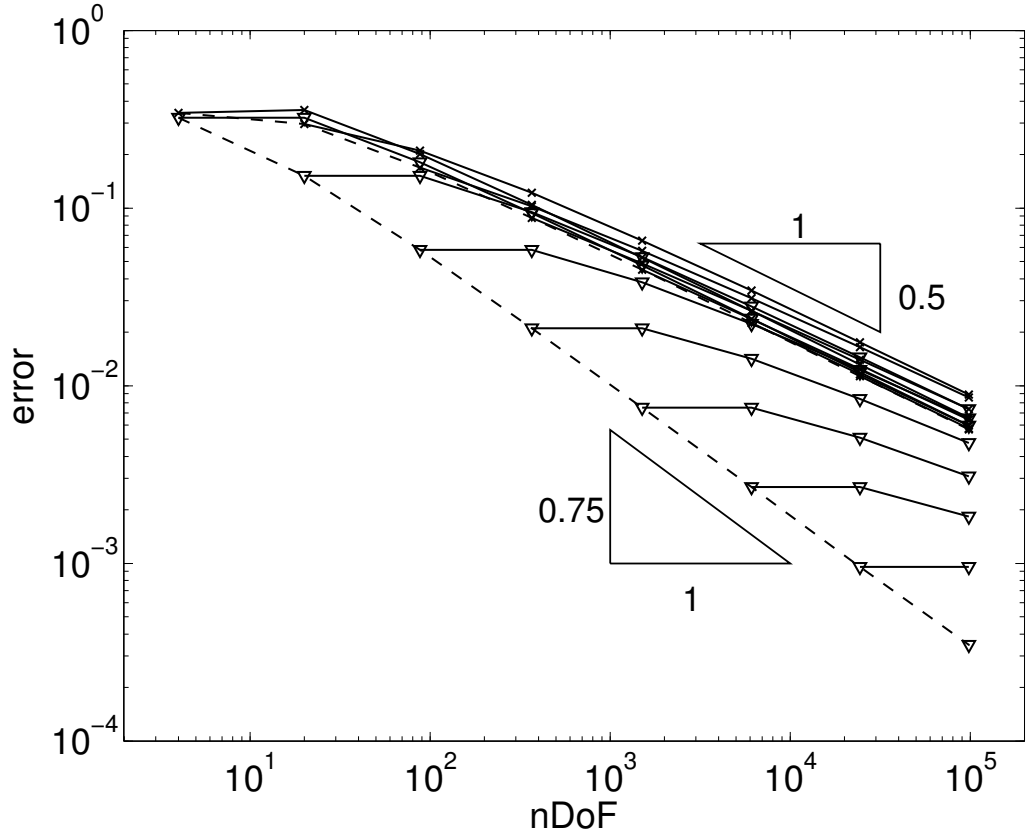

Figure 4.2: Errors of CR-NCFEM ($\times$) and RT-MFEM ($\triangledown$) in Subsection 4.1.

polygonal domain $\Omega \subset \mathbb{R}^2$ for instance, do not allow for the improved convergence of the Raviart-Thomas MFEM.

To illustrate this, let the origin 0 be a nonconvex vertex of $\partial\Omega$ with maximal interior angle ω such that, up to some smooth truncation function, the leading singular function has the form

$$u_{sing}(r,\varphi) = r^{\alpha}\,\sin(\alpha\varphi) \quad \text{for } 0 < r < 1 \text{ and } 0 < \varphi < \omega$$

with $1/2 < \alpha := \pi/\omega < 1$. Given any triangle T with vertex 0, the approximation error of the flux $\nabla u_{sing} = \alpha r^{\alpha-1}(\sin\alpha\varphi, \cos\alpha\varphi)$ by Raviart-Thomas functions is bounded from below by

$$\min_{a,b,c\in\mathbb{R}} \|\nabla u_{sing}(x) - (a,b) - cx\|_{L^2(T)} \approx h_T^{\alpha}$$

and hence is of the same order as the interpolation error of the piecewise affine nodal or edge-wise interpolation in the Courant or Crouzeix-Raviart FEM. For meshes where this defines the convergence rates like in the numerical examples below, this shows that the Raviart-Thomas MFEM has the same order of convergence and is not superior to the remaining two finite element schemes.

The L-shaped domain $\Omega = [-1,1]^2 \setminus ([0,1]\times[-1,0])$ illustrates this with the right-hand side $f \equiv 2$. The solutions of (2.1.b), (2.2.b) and (2.3.b) are computed on a sequence of red-refined triangulations $\mathcal{T}_0, \mathcal{T}_1, \ldots, \mathcal{T}_6$ and a sequence of graded meshes $\mathcal{T}_j^G$ for $j = 3, 4, 8, 16, 32, 64, 128, 256$ with grading parameter $\beta = 3/2$ where j denotes the vertices on one side of one macro triangle. The initial triangulation $\mathcal{T}_0$ for the red-refined triangulations and the graded mesh $\mathcal{T}_3^G$ are depicted in Figure 4.3. The errors for solutions on a red-refined triangulation are computed by a P_2 reference solution on $\mathcal{T}_9$ and the errors for a solution on a graded mesh $\mathcal{T}_j^G$ are computed by a P_2 reference solution on $\mathrm{red}^{(2)}(\mathcal{T}_j^G)$. Figure 4.4 reveals the expected convergence rates $1/3$ (resp. $1/2$) for uniform (resp. graded) meshes for all three methods. The equivalence of the three methods is clearly visible.

References

[1] R. Becker, S. Mao, and Z. Shi. A convergent nonconforming adaptive finite element method with quasi-optimal complexity. *SIAM J. Numer. Anal.*, 47(6):4639–4659, 2010.

[2] P. Binev, W. Dahmen, and R. DeVore. Adaptive finite element methods with convergence rates. *Numer. Math.*, 97(2):219–268, 2004.

[3] P. B. Bochev and M. D. Gunzburger. *Least-squares finite element methods*, volume 166 of *Applied Mathematical Sciences*. Springer, New York, 2009.

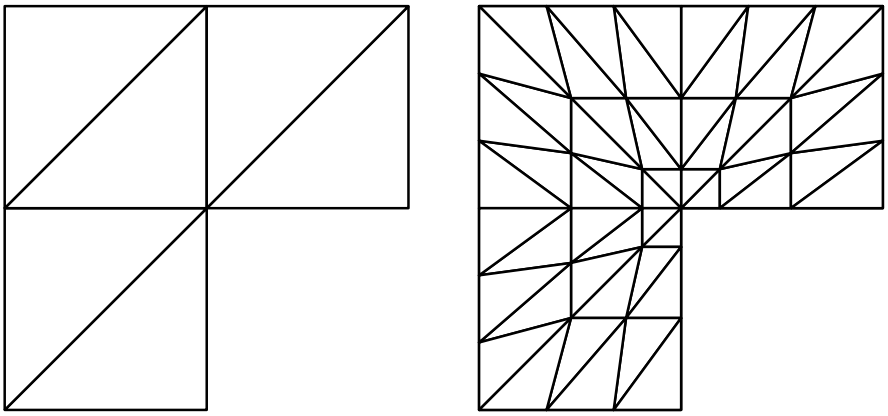

Figure 4.3: The initial triangulation for the red-refined triangulations (left) and a graded mesh (right) of the L-shaped domain from Subsection 4.2.

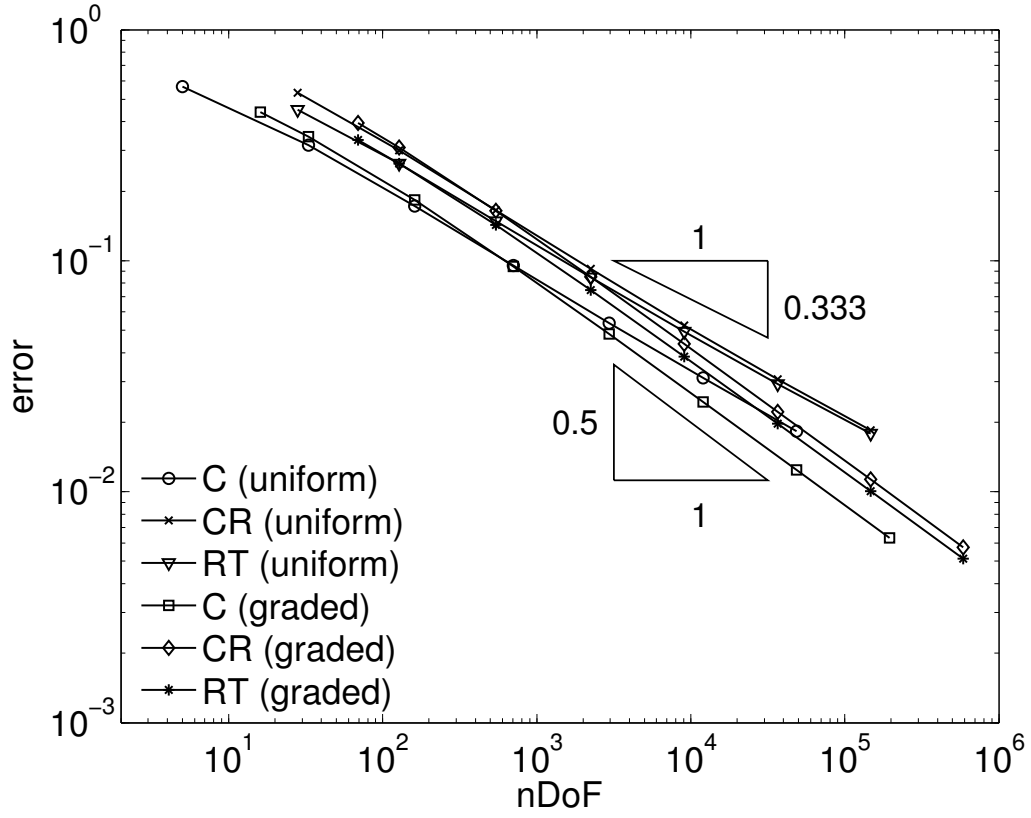

Figure 4.4: Errors of CFEM, CR-NCFEM and RT-MFEM for uniform red-refined and graded meshes on the L-shaped domain.

[4] D. Braess. *Finite elements*. Cambridge University Press, Cambridge, third edition, 2007. Theory, fast solvers, and applications in elasticity theory, Translated from the German by Larry L. Schumaker.

[5] D. Braess. An a posteriori error estimate and a comparison theorem for the nonconforming P_1 element. *Calcolo*, 46(2):149–155, 2009.

[6] J. Brandts, Y. Chen, and J. Yang. A note on least-squares mixed finite elements in relation to standard and mixed finite elements. *IMA J. Numer. Anal.*, 26(4):779–789, 2006.

[7] C. Carstensen, R. Hoppe, C. Löbhard, and M. Eigel. A review of unified a posteriori finite element error control. *IMA Preprint Series*, 2338, October 2010.

[8] C. Carstensen and H. Rabus. An optimal adaptive mixed finite element method. *Math. Comp.*, 2009. In press.

[9] J. Cascon, C. Kreuzer, R. H. Nochetto, and K. G. Siebert. Quasi-optimal convergence rate for an adaptive finite element method. *SIAM J. Numer. Anal.*, 46(5):2524–2550, 2008.

[10] L. Chen, M. Holst, and J. Xu. Convergence and optimality of adaptive mixed finite element methods. *Math. Comp.*, 78(265):35–53, 2009.

[11] R. Courant. On a method for the solution of boundary-value problems. In *Theodore von Kármán Anniversary Volume*, pages 189–194. California Institue of Technology, Pasadena, Calif., 1941.

[12] M. Crouzeix and P.-A. Raviart. Conforming and nonconforming finite element methods for solving the stationary Stokes equations. I. *Rev. Française Automat. Informat. Recherche Opérationnelle Sér. Rouge*, 7(R-3):33–75, 1973.

[13] E. Dari, R. Duran, C. Padra, and V. Vampa. A posteriori error estimators for nonconforming finite element methods. *RAIRO Modél. Math. Anal. Numér.*, 30(4):385–400, 1996.

[14] T. Gudi. A new error analysis for discontinuous finite element methods for linear elliptic problems. *Math. Comp.*, 79(272):2169–2189, 2010.

[15] J. Ku. Weak coupling of solutions of first-order least-squares method. *Math. Comp.*, 77(263):1323–1332, 2008.

[16] L. D. Marini. An inexpensive method for the evaluation of the solution of the lowest order Raviart-Thomas mixed method. *SIAM J. Numer. Anal.*, 22(3):493–496, 1985.

[17] H. Rabus. A natural adaptive nonconforming FEM of quasi-optimal complexity. *Comput. Methods Appl. Math.*, 10(3):315–325, 2010.

[18] P.-A. Raviart and J. M. Thomas. A mixed finite element method for 2nd order elliptic problems. In *Mathematical aspects of finite element methods (Proc. Conf., Consiglio Naz. delle Ricerche (C.N.R.), Rome, 1975)*, pages 292–315. Lecture Notes in Math., Vol. 606. Springer, Berlin, 1977.

[19] R. Verfürth. *A review of a posteriori error estimation and adaptive mesh-refinement techniques*. Advances in numerical mathematics. Wiley-Teubner, 1996.